2023

A Facile Strategy for the Fabrication of Cell-Laden Porous Alginate Hydrogels based on Two-Phase Aqueous Emulsions

Wen Xue

Donghee Lee

Yunfan Kong

Mitchell A. Kuss

Ying Huang

See next page for additional authors

Authors

Wen Xue, Donghee Lee, Yunfan Kong, Mitchell A. Kuss, Ying Huang, Taesung Kim, Soonkyu Chung, Andrew T. Dudley, Seung-hyun Ro, and Bin Duan

ADVANCED FUNCTIONAL MATERIALS
www.afm-journal.de

A Facile Strategy for the Fabrication of Cell-Laden Porous Alginate Hydrogels based on Two-Phase Aqueous Emulsions

Wen Xue, Donghee Lee, Yunfan Kong, Mitchell Kuss, Ying Huang, Taesung Kim, Soonkyu Chung, Andrew T. Dudley, Seung-Hyun Ro, and Bin Duan**

Porous alginate (Alg) hydrogels possess many advantages as cell carriers. However, current pore generation methods require either complex or harsh fabrication processes, toxic components, or extra purification steps, limiting the feasibility and affecting the cellular survival and function. In this study, a simple and cell-friendly approach to generate highly porous cell-laden Alg hydrogels based on two-phase aqueous emulsions is reported. The pre-gel solutions, which contain two immiscible aqueous phases of Alg and caseinate (Cas), are cross-linked by calcium ions. The porous structure of the hydrogel construct is formed by subsequently removing the Cas phase from the ion-cross-linked Alg hydrogel. Those porous Alg hydrogels possess heterogeneous pores ≈100 µm and interconnected paths. Human white adipose progenitors (WAPs) encapsulated in these hydrogels self-organize into spheroids and show enhanced viability, proliferation, and adipogenic differentiation, compared to non-porous constructs. As a proof of concept, this porous Alg hydrogel platform is employed to prepare core-shell spheres for coculture of WAPs and colon cancer cells, with WAP clusters distributed around cancer cell aggregates, to investigate cellular crosstalk. This efficacious approach is believed to provide a robust and versatile platform for engineering porous-structured Alg hydrogels for applications as cell carriers and in disease modeling.

1. Introduction

Alginate (Alg) is a natural polysaccharide that has been extensively investigated and used for various biomedical applications due to its biocompatibility, low cost, and mild gelation by divalent cations, like calcium and barium ions.[1] The structural similarity of Alg hydrogels to tissue extracellular matrices (ECMs) allows them to have wide applications as cell carriers, including cell delivery, disease modeling, and tissue regeneration.[1b] In these fields, the pore size of the Alg hydrogel is one of the most important parameters because it regulates oxygen and solute transportation properties in and out of hydrogels, controls encapsulated cell migration and interaction, and further affects cellular retention and function.[2] Normally, the hydrogel pore size is on the nanometer scale, defined as the distance of cross-linked polymer chains within hydrogel networks.[3] Such pore size allows for diffusion of small molecules. However, it limits the transportation of some macromolecules,

W. Xue
College of Biological Science and Medical Engineering
Donghua University
Shanghai 201620, China

W. Xue, Y. Kong, M. Kuss, B. Duan
Department of Internal Medicine
University of Nebraska Medical Center
Omaha, NE 68198, USA
E-mail: bin.duan@unmc.edu

W. Xue, D. Lee, Y. Kong, M. Kuss, A. T. Dudley, B. Duan
Mary & Dick Holland Regenerative Medicine Program
University of Nebraska Medical Center
Omaha, NE 68198, USA

D. Lee, B. Duan
Department of Surgery
University of Nebraska Medical Center
Omaha, NE 68198, USA

Y. Huang
Eppley Institute for Research in Cancer and Allied Diseases
University of Nebraska Medical Center
Omaha, NE 68198, USA

T. Kim, S.-H. Ro
Department of Biochemistry and the Redox Biology Center
University of Nebraska-Lincoln
Lincoln, NE 68588, USA
E-mail: shro@unl.edu

S. Chung
Department of Nutrition
University of Massachusetts Amherst
Amherst, MA 01003, USA

A. T. Dudley
Department of Genetics
University of Nebraska Medical Center
Omaha, NE 68198, USA

B. Duan
Department of Mechanical and Materials Engineering
University of Nebraska-Lincoln
Lincoln, NE 68588, USA

The ORCID identification number(s) for the author(s) of this article can be found under https://doi.org/10.1002/adfm.202214129

DOI: 10.1002/adfm.202214129

migration and proliferation of encapsulated cells, and infiltration of host cells, which are on the order of tens of micrometers.[4] Many previous studies have shown that micro-porous hydrogels possess many advantages in cell culture over their nano-porous counterparts. For example, micro-porous biomaterials were illustrated to improve the survival of transplanted cells, provide molecular cues to direct cellular phenotypes, and enhance tissue regeneration.[2,5] Also, it has been suggested that micro-porous hydrogels have the potential to form cell spheroids in situ,[6] which are multi-cellular aggregates that have better biological properties, superior metabolic functions, and improved viability compared to dispersed cells.[7] Thus, there is a critical need for the development of porous Alg hydrogel constructs as cell carriers.

Several methods have been explored to generate Alg hydrogels with pore sizes in the micrometer range. The sacrificial template method is the most frequently used technique for creating porous Alg structures. The templates applied include removable solid particles, like calcium carbonate ($CaCO_3$) crystals and gelatin beads;[8] oil emulsions;[9] and gas bubbles.[9b,10] Alg hydrogels are cross-linked in media mixed with those templates, and the templates are subsequently leached out, creating hydrogels with pore sizes that match the templates. However, all these approaches have some limitations. For the solid templates, one notable disadvantage of $CaCO_3$ crystals is the high osmotic pressure generated during the dissolution of $CaCO_3$, which leads to encapsulated cell death, and degradable gelatin particles require extra steps for fabrication and collection. Although oil emulsifications are simple and don't need extra steps, the immiscible organic solvents involved are incompatible with cell survival and are difficult to totally remove. For the gas formation, sodium bicarbonate is one of the most widely used gas foaming agents because it generates carbon dioxide in acidic conditions,[11] but it still poses challenges in terms of cell viability. Freeze-drying is another commonly used method for creating pores. However, cells have to be seeded after porous scaffold formation, limiting their homogeneous distribution and infiltration throughout the scaffolds.[8a] Therefore, there is still an unmet need for porous Alg hydrogels that can encapsulate cells and be fabricated under cyto-compatible conditions.

One attractive application of cell-laden Alg hydrogels is to serve as in vitro disease models to understand pathological mechanisms.[12] For cancer-associated diseases, mounting evidence has shown that adipocytes and adipose tissues play pivotal roles in tumor initiation, progression, and metastasis.[13] Peritumoral white adipose tissue adjacent to malignant cells was revealed to have smaller lipid droplets than those away from the tumor.[14] Carcinomas were also found to invade adjacent adipose tissues.[14a,15] To address the interactions between adipocytes and cancer cells, identify pathological responses, and discover potential therapeutic targets, physiologically relevant in vitro disease models are extremely needed. 2D coculture models with cells seeded in a transwell or treated with conditioned medium may oversimplify the process, and such indirect cell contact cannot recapitulate in vivo environments.[16] 3D coculture models with direct cell contact are more effective. Most current 3D coculture models are generated through mixing monodispersed adipocytes and tumor cells together in hydrogels.[17] However, they suffer from the significant limitation of losing the spatial structure of native tissues, where tumor cell aggregates interact with adipocyte clusters. In addition, it is challenging to investigate the influence of the coculture on each cell type. Instead, most previous studies treated the cocultured system as a whole and investigated the overall effects.[17]

To address limitations mentioned above, we report a simple and cell-friendly strategy to generate highly porous, cell-laden Alg hydrogels and the evaluation toward their feasibility for use in adipocyte-cancer cell coculture applications. We hypothesize that bioinert Alg hydrogels with micron-sized pores can improve encapsulated cell survival and facilitate in situ formation of cell spheroids to mimic native tissues. To test this hypothesis, we first fabricated porous Alg hydrogels with heterogeneous pores and interconnected paths based on Alg/caseinate (Cas) aqueous emulsions at room temperature. The morphological, mechanical, and macromolecule diffusion properties of the porous hydrogels were then evaluated. Further, as a proof of concept, human white adipose progenitor cells (WAPs) were encapsulated to verify the biocompatibility of the porous Alg hydrogels and investigate the self-organization of WAPs into spheroids. Later, the differentiation behaviors of WAP spheroids in porous Alg hydrogels were compared with monodispersed WAPs in non-porous Alg hydrogels. Finally, core–shell porous Alg spheres were prepared to study the WAP-colon cancer cell coculture, with WAP clusters distributed around cancer cell aggregates. Overall, we propose an innovative and efficacious approach for fabricating porous Alg constructs for use as cell carriers that improve cell viability, functionality, and spheroid formation.

2. Results and Discussion

2.1. Preparation of Immiscible Alg/Cas Emulsions

The present study intends to develop novel porous Alg hydrogels with highly interconnected porous structures that can be used as cell carriers. We took advantage of two-phase aqueous emulsions consisting of Alg and Cas for the fabrication of the hydrogels. Cas is a major protein in milk and is highly biocompatible.[18] Within a certain concentration range, aqueous Alg and Cas solutions are not miscible, creating a system with droplets of one immiscible phase dispersed within the other continuous aqueous phase.[19] This aqueous phase separation between Alg and Cas is due to the thermodynamic incompatibility of proteins and polysaccharides.[19] After the polymerization of Alg, Cas droplets will be dissolved, generating highly interconnected pores in the Alg matrix. The whole fabrication process is mild, biocompatible, and maintained in an aqueous environment. A readily tunable pore size can be achieved by two-phase volume ratios.

The immiscible Alg/Cas emulsions were first prepared by mixing and dissolving Alg and Cas in saline (**Figure 1**A–i). The phase diagram of Alg/Cas binary mixture was shown in Figure S1 (Supporting Information). In order to ensure adequate mechanical support and successful gelation of Alg hydrogels, 2% Alg was chosen as the base according to our preliminary experiments, and Cas concentrations ranging from 1% to 5% were introduced (higher concentration Cas cannot dissolve well). With the increase of the Cas concentration, larger droplets were dispersed in the continuous phase (Figure 1B). At the same time, the inclusion of Cas increased the Alg viscosity (Figure 1C), with the

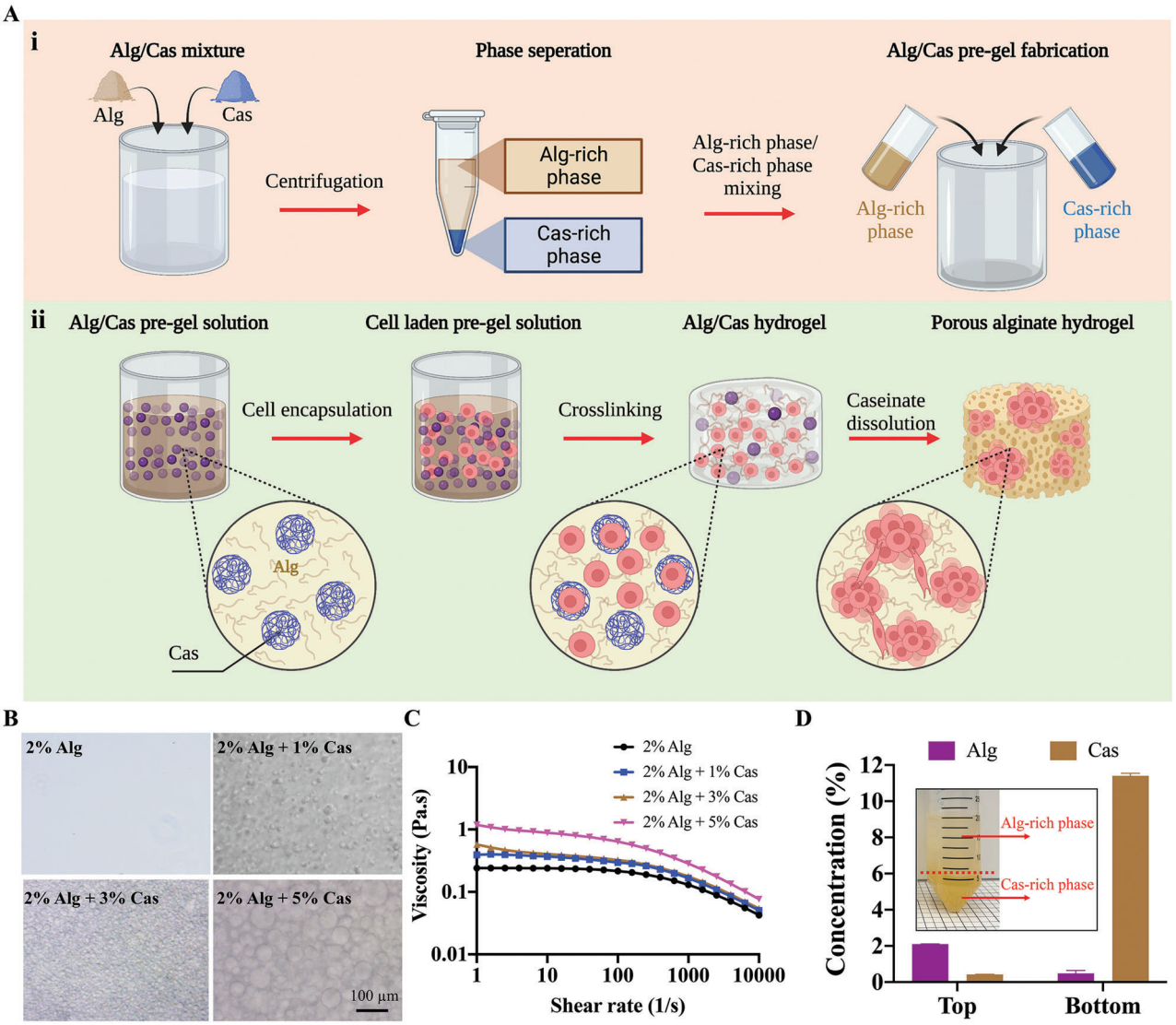

Figure 1. Preparation of Alg/Cas emulsions. A) Schematic showing the fabrication process of porous cell-laden Alg hydrogels based on Alg/Cas emulsions. A-i: Alg and Cas are mixed and centrifuged to separate the Alg-rich and Cas-rich phases. Different volume ratios of the Alg-rich phase/Cas-rich phase mixture is applied for the formation of pre-gel solutions. A-ii: Cells are encapsulated into pre-gel solutions before hydrogel cross-linking. With the dissolution of Cas, porous Alg hydrogels form, and cells self-organize into spheroids. B) Optical images of Alg/Cas emulsions as the Cas concentration varies from 0% to 5%. C) Viscosity of Alg/Cas emulsions, with Cas concentration varying from 0% to 5%. D) Semi-quantitative evaluation of the composition of the Alg-rich and Cas-rich phases.

addition of 5% Cas showing the highest values. The solution with a high viscosity is stable and can prevent the phases from separating before being cross-linked.[20] Also, viscous solutions with encapsulated cells can slow down the cell sedimentation process, facilitating a homogenous cell distribution. Thus, to ensure stable Alg/Cas emulsions, 2% Alg mixed with 5% Cas was chosen for the following experiments.

The Alg/Cas emulsions obtained were centrifuged to separate the mixture into two phases, namely the Alg-rich phase and Cas-rich phase (Figure 1A–i). This step could improve the flexibility of tuning the droplet sizes of the emulsion by adjusting the volume ratios of the separated phases, which significantly benefits polymers with low solubilities. According to the semi-quantitative evaluations, the top phase was Alg-rich, while the bottom phase was Cas-rich (Figure 1D). Note that the Alg-rich phase was different from the Alg phase because it also contained some Cas polymers, which also occurred with Alg in Cas-rich phase. Also, the Alg-rich and Cas-rich phases obtained after centrifugation were completely immiscible, while the Alg and Cas phases were partially miscible.

2.2. Fabrication and Characterization of Porous Alg Hydrogels

To fabricate porous Alg hydrogels, we prepared pre-gel solutions by mixing various volume ratios of the Alg-rich phase and Cas-rich phase, from 0:100 to 100:0 (Figure 1A–i). The pre-gel solutions were imaged under an optical microscope and a confocal

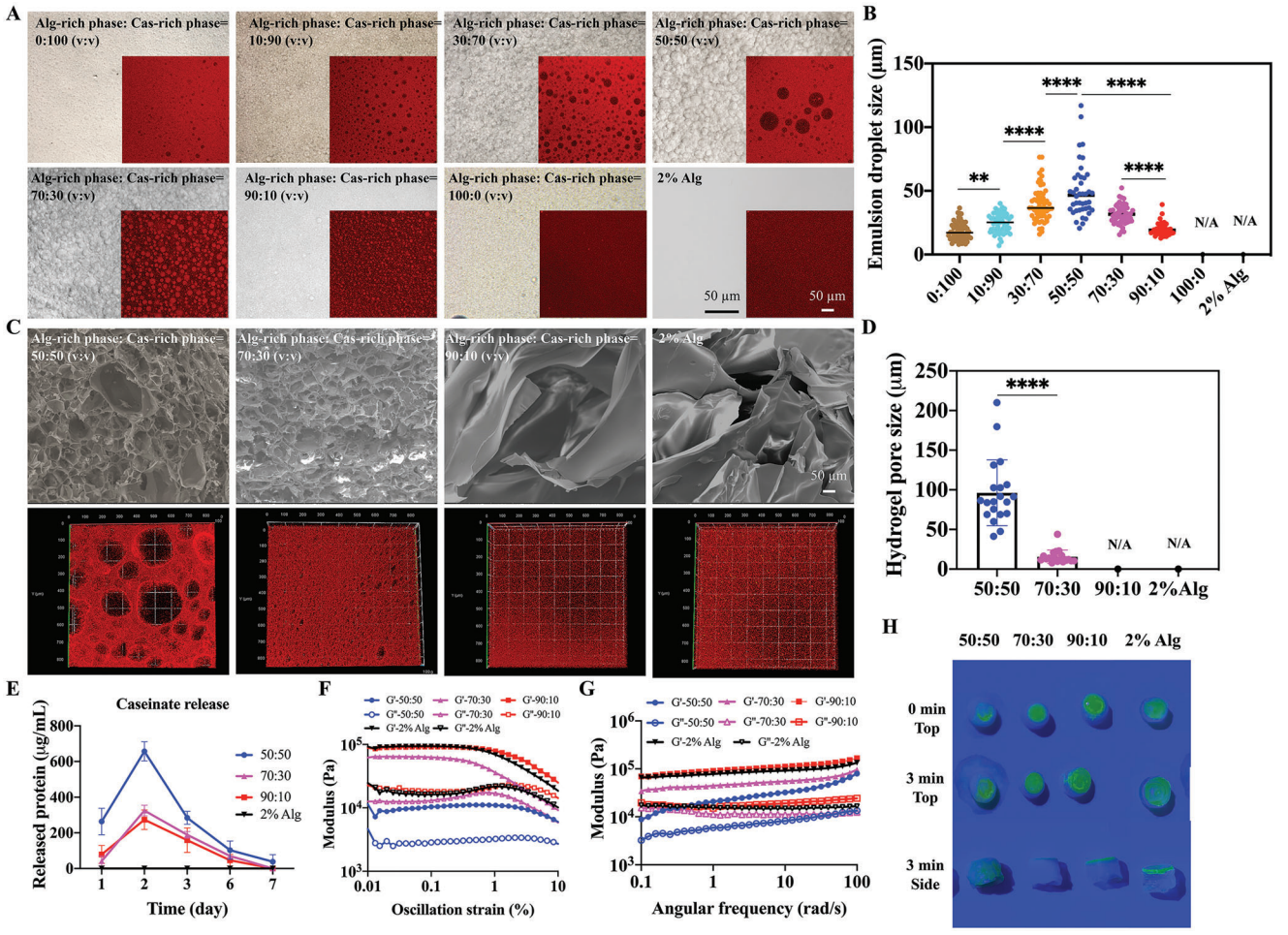

Figure 2. Characterization of Alg/Cas pre-gel solutions and porous Alg hydrogels. A) Optical and fluorescent images of pre-gel solutions with various Alg-rich phase to Cas-rich phase volume ratios. Alg was conjugated by tetramethylrhodamine for the fluorescent images. B) Emulsion droplet sizes in Alg/Cas pre-gel solutions (n = 40–60). C) SEM and 3D reconstruction confocal fluorescence images showing the Alg hydrogels with interconnected pores. D) Pore size distribution in different Alg hydrogels (n = 20). 90:10 volume ratio and 2% alginate hydrogels showed undetectable porous structures. E) Release of Cas from Alg/Cas hydrogels over time. F) Storage and loss modulus of Alg hydrogels under an oscillation strain sweep. G) Storage and loss modulus of Alg hydrogels under an angular frequency sweep. H) FITC-conjugated dextran diffusion through Alg hydrogels. All quantitative data are expressed as the mean ± standard deviation. Asterisks indicate statistically significant comparisons, with $^{**}p < 0.01$ and $^{****}p < 0.0001$, by Student's t-test or one-way ANOVA with Tukey's multiple comparisons tests.

laser scanning microscope (CLSM), with Alg labeled by tetramethylrhodamine cadaverine (red fluorescence dye). When the volume ratio of the Alg-rich phase to the Cas-rich phase was increased from 0:100 to 50:50, Cas droplets (dark voids) were dispersed in the Alg continuous phase (red phase) with increasing sizes (**Figure 2**A). When further increasing the Alg-rich phase volume ratio, we observed Alg droplets with decreasing sizes dispersed in the continuous phase (Figure 2A). Pre-gel solutions with 100:0 volume ratio and 2% Alg illustrated homogenous state without droplets dispersed (Figure 2A). The emulsion droplet sizes in pre-gel solutions were evaluated, and they ranged from 18 ± 7 to 50 ± 21 μm by changing the phase volume ratios (Figure 2B). This tunable droplet sizes led to tunable pore sizes in cross-linked hydrogels.

Furthermore, Alg/Cas pre-gel solutions were cross-linked by calcium ions (calcium chloride, $CaCl_2$) to fabricate Alg hydrogels containing Cas droplets. When exposed to calcium ions, some pre-gel solutions with relatively low Alg-rich phase ratios were unable to solidify and gelate (i.e., Alg-rich phase: Cas-rich phase = 0:100, 10:90, and 30:70). In conditions that formed hydrogels (i.e., Alg-rich phase: Cas-rich phase = 50:50, 70:30, 90:10, 100:0, 2% Alg, Figure S2, Supporting Information), porous structures were evaluated morphologically by a scanning electron microscope (SEM, with lyophilization) and a CLSM (without lyophilization) (Figure 2C). SEM imaging clearly illustrated heterogeneous pores in the 50:50 and 70:30 hydrogels (Figure 2C). However, 90:10 and 2% Alg showed lamellar structures from lyophilization. According to the CLSM imaging, hydrogels with ratios of 50:50 and 70:30 showed dark voids (pores) within red stained Alg networks, while 90:10 and 2% Alg appeared to be homogeneous structures with undetectable dark voids. To quantitatively analyze the size distribution of pores dispersed in Alg hydrogels, ImageJ software was applied with the CLSM images. The average pore size decreased from 97 ± 40 to 15 ± 8 μm as the

volume ratio of the Alg-rich phase increased from 50:50 to 70:30 (Figure 2D).

The release profile of Cas from Alg hydrogels into the solution was examined. As shown in Figure 2E, the Cas release peaked at day 2 and then decreased over time. At day 7, almost no Cas residue was detected in the solution. The rheological properties of fabricated hydrogels were evaluated by oscillation strain sweep and frequency sweep (Figure 2F,G). It was found that, after ionic cross-linking, all hydrogels illustrated higher storage moduli than their loss moduli, indicating successful gelation. Standard 2% Alg and 90:10 ratio hydrogels had comparable storage moduli and loss moduli. The introduction of porous structures within Alg hydrogels decreased their moduli. The hydrogels with the largest pore size (50:50) had the lowest storage modulus values compared to their counterparts, which may help encapsulated cell remodeling behaviors. The ability of macromolecules, like fluorescein isothiocyanate (FITC)-conjugated-dextran and bovine serum albumin (BSA), to diffuse through the porous hydrogels was investigated. It was observed that FITC-conjugated-dextran could diffuse quickly through hydrogels with large pore sizes (50:50), but not the 70:30, 90:10, or 2% Alg hydrogels (Figure 2H). FITC-conjugated-dextran was clearly detected on the filter paper as well as on the sides of the 50:50 ratio hydrogel after 3 min (Figure 2H). Similar results were shown by BSA diffusion, with hydrogels put on a petri dish (Figure S3, Supporting Information).

2.3. In Situ Formation of WAP Spheroids within Porous Alg Hydrogels

The bioinertness of Alg polymers restricts cell-matrix interactions, which limits some applications of Alg as a cell carrier. However, limited cell-matrix interactions in porous Alg hydrogels can facilitate cell migration, cell-cell interactions, and in situ cell spheroid generation. Here, WAPs were suspended in the aforementioned Alg/Cas pre-gel solutions (Figure 1A-ii). Then the WAP-laden hydrogels were successfully fabricated by calcium ion cross-linking. Hydrogels with large pore size (Alg-rich phase: Cas-rich phase = 50:50), small pore size (Alg-rich phase: Cas-rich phase = 70:30), homogeneous structures (Alg-rich phase: Cas-rich phase = 90:10), and 2% Alg control were investigated here. We expected that, with the Cas phase leaching out and generating a porous structure, WAPs would proliferate and migrate to connect with each other and form spheroids in situ.

The WAP viability was characterized by a Live/Dead assay at days 0, 3, and 7 to record the spheroid formation process (**Figure 3**A). At day 0, all cells were homogenously distributed within all groups of hydrogels. However, at day 3, large numbers of WAPs started to aggregate with each other in the 50:50 ratio hydrogels, and several cells gathered in the 70:30 ratio hydrogels (Figure 3A). At day 7, WAPs in hydrogels with large pore sizes (50:50) aggregated closely and formed spheroids with diameters of ≈100 μm inside the hydrogels. In porous hydrogels with smaller pore sizes (70:30), multiple cells gathered and formed small cell clusters (Figure 3A). In contrast, WAPs dispersed uniformly in 90:10 ratio and 2% Alg hydrogels without aggregation during the culture time (Figure 3A). We also semi-quantitatively evaluated cell or cell cluster areas in hydrogels based on Live/Dead images. The cell cluster area increased over time in the 50:50 ratio hydrogels and was significantly higher than their counterparts (Figure 3B). A statistical difference was also noticed between cell clusters in 70:30 ratio hydrogels and dispersed cells in 90:10 and 2% Alg hydrogels (Figure 3B). Bright-field images and Hematoxylin and Eosin (H&E) staining confirmed successful formation of spheroids in 50:50 hydrogels, small cell clusters in 70:30 hydrogels, and individual cell distribution in 90:10 and 2% Alg hydrogels (Figure 3C,D). WAP proliferation was significantly enhanced after the incorporation of Cas compared to the 2% Alg hydrogel, probably due to the biologically active properties of Cas and the formation of porous structures (Figure 3E). However, 70:30 and 90:10 hydrogels had higher MTT values than that of 50:50 hydrogels. It was speculated that Cas leaching might take some cells out of the 50:50 ratio hydrogels, leading to relatively lower cellular numbers.

Porous hydrogels are of strong interest for biomedical applications related to cell incorporation, as their passageways maximize the transport ability and enable fast cellular infiltration and interaction. Porous structures and bioinert polymer skeletons are two important factors of cell-laden hydrogels for efficiently and directly producing cell spheroids in situ (Figure 3F). Without the porous structure, encapsulated cells have limited migration and spreading space in bioinert matrices and are individually dispersed (Figure 3F). For porous hydrogels with cell adhesion domains, like gelatin, encapsulated cells illustrate strong cell-cell and cell-matrix interactions without forming cellular clusters.[5b] However, in the bioinert porous hydrogels, like Alg, cell-matrix crosstalk is restricted, thus cells prefer aggregating and interacting with each other strongly to form spheroids (Figure 3F). Spheroids have an in vivo-like microenvironment, allowing cells to further interact within their secreted ECMs. Cells in spheroids have also been reported to have enhanced survival and differentiation ability as well as augmented angiogenic and anti-inflammatory cytokines secretion.[21] Besides, here in our study, WAP spheroids can better mimic the physiological adipose tissues, which are composed of adipocytes in round shape and aggregating closely like clusters.

2.4. Improved WAP Adipogenic Differentiation in Porous Alg Spheres

We have proved that WAPs could successfully aggregate into spheroids in porous Alg hydrogels. Here, whether porous structures and spheroids would improve WAP adipogenic differentiation was investigated in Alg spheres. Spheres possess many advantages in biomedical applications over other geometries. For example, they have large surface areas that allow for sufficient host tissue integration, can be injected, and have versatile processabilities that allow them to be engineered into multiple constructs.[22] Two pre-gel recipes mentioned previously were chosen. One is the Alg-rich to Cas-rich phase volume ratio as 50:50, which formed porous hydrogels. The other is the 2% Alg solution, which works as the non-porous control.

Our previously reported 3D printed device was applied to generate Alg spheres in high throughput.[23] Pre-gel solutions were injected through the syringe and broken into droplets by the air flow. They were then collected and cross-linked in $CaCl_2$

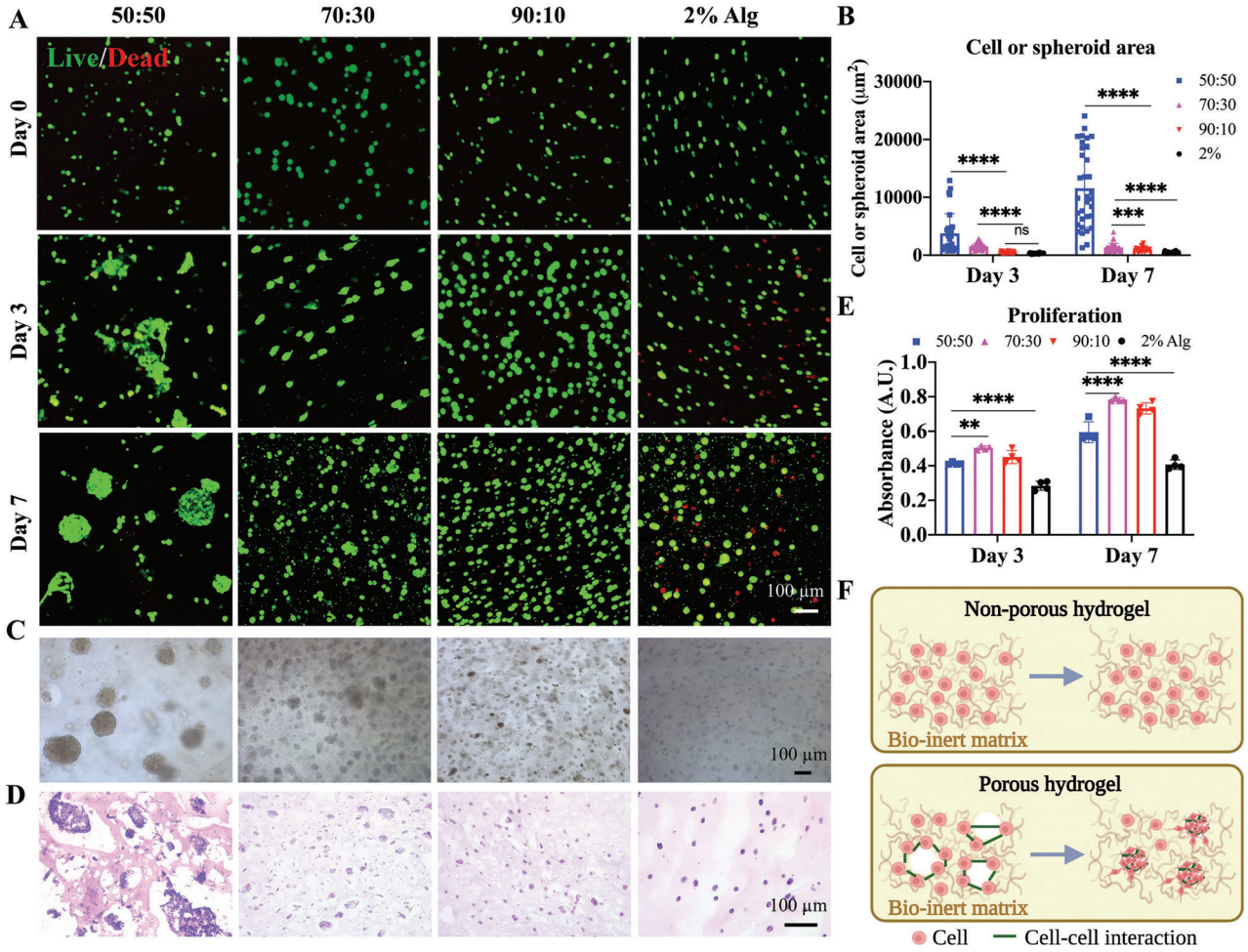

Figure 3. In situ WAP spheroid formation in porous Alg hydrogels. A) Live/Dead assay of WAPs in Alg hydrogels. B) WAP or WAP spheroid areas in Alg hydrogels at days 3 and 7 (n = 30-40). C) Optical images showing encapsulated WAPs at day 7. D) H&E staining of WAPs in hydrogels at day 7. E) Quantifications of the proliferation of WAPs in hydrogels at days 3 and 7 using MTT (n = 4). F) Schematic showing the spheroid formation process in a porous hydrogel with a bioinert matrix. All quantitative data are expressed as the mean ± standard deviation. Asterisks indicate statistically significant comparisons, with $^{**}p < 0.01$, $^{***}p < 0.001$, and $^{****}p < 0.0001$, by Student's t-test or one-way ANOVA with Tukey's multiple comparisons tests.

solutions, forming Alg spheres instantly. This process was quick and biocompatible as well as high throughput. We first evaluated the morphology of the Alg spheres without cell encapsulation. All spheres were uniform in size, with average diameter of 1.28 mm for 50:50 spheres and 1.30 mm for 2% Alg spheres (**Figure 4**A; Figure S4, Supporting Information). The 50:50 spheres looked milky white, which came from Cas, while 2% Alg spheres were transparent. SEM images demonstrated interconnected pore structures within the 50:50 spheres and a lamellar-like morphology in 2% Alg spheres, which may originate from lyophilization (Figure 4A). WAPs were then suspended in pre-gel solutions to fabricate WAP-laden spheres. After 7 days of culture in the medium, the Cas phase leached out from the spheres, and they transitioned from milky white to transparent (Figure 4B). Brightfield images were taken, and WAPs aggregated with each other to form spheroids within 50:50 spheres. Individually distributed cells were observed in 2% Alg spheres (Figure 4B). The Live/Dead assay confirmed spheroid formation and high cell viability in 50:50 porous spheres, while many cells were dead in 2% Alg spheres, most likely due to poor transportation of nutrients and oxygen. MTT absorbance showed a significantly higher proliferation of WAPs cultured in porous spheres than those in non-porous Alg ones (Figure 4C).

Besides enhanced survival and proliferation of WAP spheroids in porous Alg spheres, more effective adipogenic differentiation, indicated by accumulated lipids and ECM deposition, was also observed. Quantitative analysis of the intracellular triglyceride concentration was evaluated and compared for WAPs in porous and non-porous Alg spheres with and without adipogenic differentiation. Porous Alg spheres illustrated distinctively higher triglyceride concentration, reflecting more lipid contents after differentiation, compared to their counterparts (Figure 4D). Triglyceride concentrations were low and had no significant difference in 2% Alg spheres with or without differentiation. It was noted that WAPs encapsulated in porous Alg spheres accumulated more lipids, even without differentiation, than those in 2% Alg spheres, indicating possible auto-differentiation of WAP spheroids in porous hydrogels. The findings were corroborated by BODIPY and Oil Red O staining, with 50:50 porous spheres, with and without adipogenic differentiation, showing

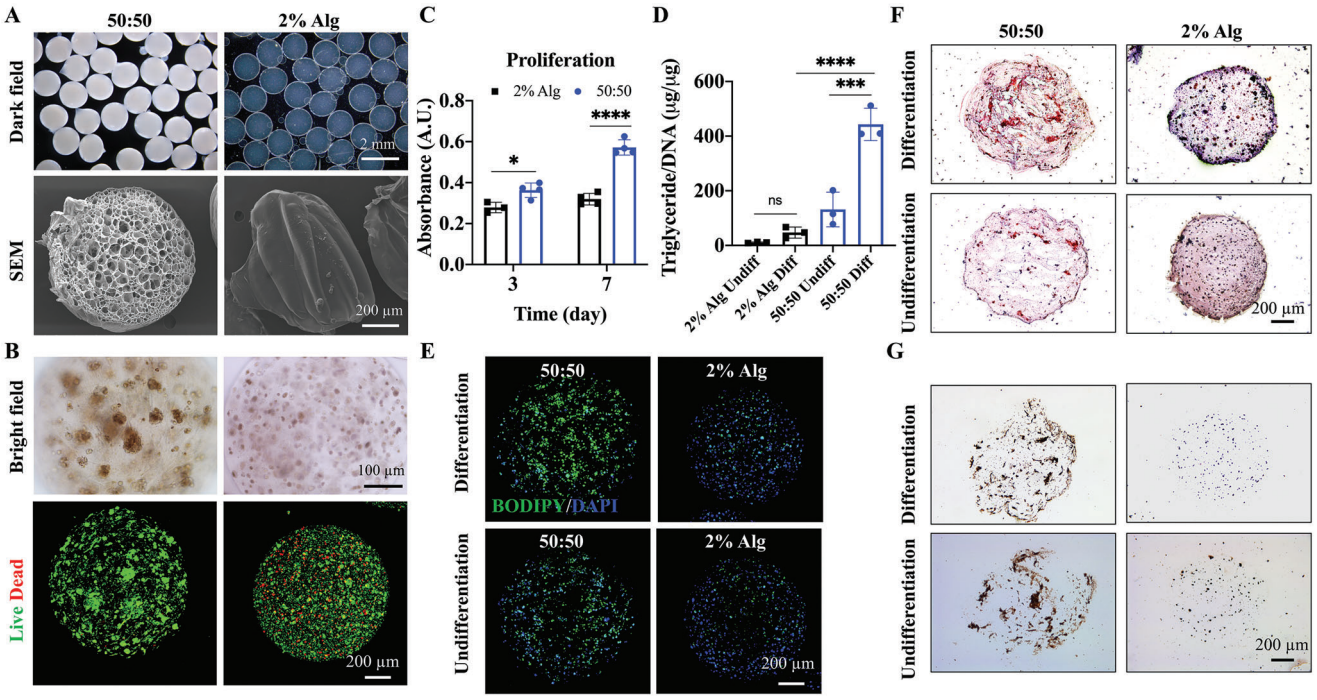

Figure 4. Characterization of cell-laden porous Alg spheres. A) Dark field and SEM images showing the morphology and microstructures of porous and control alginate spheres. B) Optical images and Live/Dead assay of WAPs encapsulated in Alg spheres at day 7. C) Quantifications of the proliferation of WAPs at days 3 and 7 using an MTT assay (n = 3-4). D) Quantifications of triglyceride concentrations in porous and standard Alg spheres with and without differentiation (n = 3). E) Lipid staining by BODIPY in porous and standard Alg spheres. F) Lipid staining by Oil Red O in porous and standard Alg spheres. G) ECM staining of collagen I in porous and standard Alg spheres. All quantitative data are expressed as the mean ± standard deviation. Asterisks indicate statistically significant comparisons, with *$p < 0.05$, ***$p < 0.001$, and ****$p < 0.0001$, by Student's t-test or one-way ANOVA with Tukey's multiple comparisons tests.

substantial dye-positive lipid droplets in the whole spheres (Figure 4E) or sphere sections (Figure 4F). Dispersed and much fewer lipids were observed in 2% Alg spheres, especially in those without differentiation (Figure 4E,F).

The development of the tissue-related ECM is considered to be an important feature in 3D tissue constructs, especially for in vitro model systems. WAP-laden spheres were immunohistochemically stained with collagen I, which is one of the major ECM components in adipose tissue. As shown in Figure 4G, WAPs in 50:50 porous spheres demonstrated high expressions of brown-positive collagen I even without differentiation, while it was rarely observed in 2% Alg spheres.

Taken together, WAPs encapsulated in porous Alg spheres spontaneously aggregated into spheroids within 7 days of culture. These spheroids improved the WAPs' survival, proliferation, and differentiation, evidenced by accumulated lipids and tissue-specific ECM deposition. In addition, WAPs in the form of spheroids could undergo auto-differentiation without treatment with differentiation medium, which was beneficial for coculture with other cells because the side effects of differentiation medium to other cells can be avoided.

2.5. WAP/Caco2 Coculture in Core-Shell Porous Alg Spheres

Adipocytes play important roles in tumor initiation, progression, and metastasis.[13] To better understand the underlying mechanisms, it is necessary to generate a disease model that addresses the interactions between adipocytes and cancer cells. At present, pre-clinical in vivo models that use orthotopic cancer cell inoculation are routinely applied.[24] Although useful, these in vivo models are in high costs and time-consuming. Therefore, in vitro adipocyte and cancer cell coculture models could be an effective tool to mimic native interactions between adipose and cancer tissues. 3D models have been developed to recapitulate the in vivo environment and are widely considered to be superior to 2D models. Most current 3D coculture models are based on mixing monodispersed adipocytes and tumor cells directly.[17] However, adipose tissue depots are situated in close proximity to the colon tissue rather than being uniformly dispersed among colon tumor cells in vivo.[25] Therefore, existing 3D models are difficult to accurately replicate the native spatial characteristics of adipocytes surrounding tumor cell aggregates. Moreover, current 3D models do not allow for the independent investigation of coculture's impact on each cell type.

To address these issues, we took advantage of core-shell structures and fabricated core-shell spheres to heterogeneously coculture WAPs and colon cancer cells. Porous Alg hydrogel platform was applied and worked as the shell, which could cross-link quickly and help produce WAP spheroids, surrounding and interacting with the cancer cell aggregates in the core. Our goal was to replicate the spatial and structural characteristics of tumors and surrounding adipocytes in physiological microenvironments. Unlike traditional core-shell spheres with nano-porous

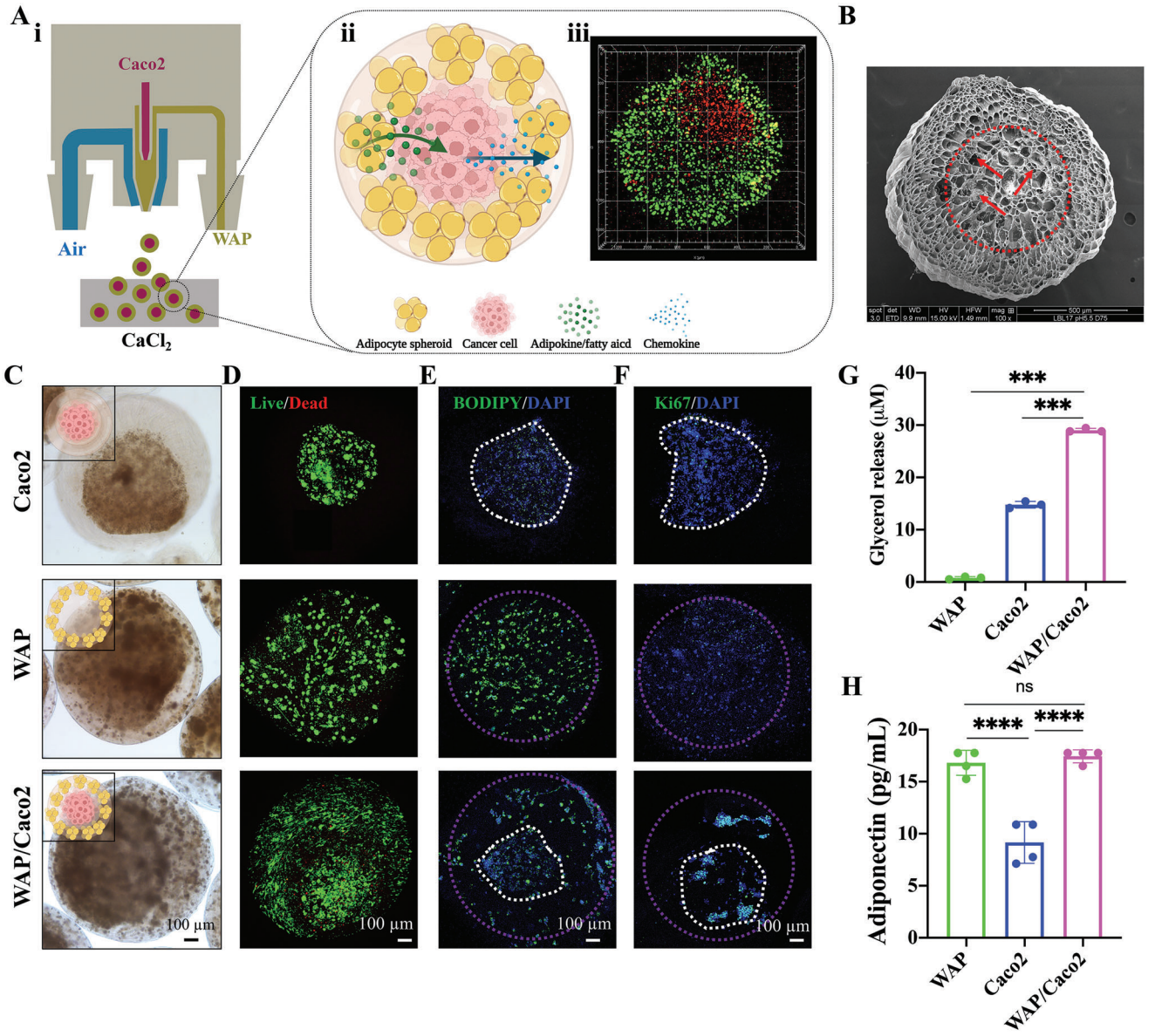

Figure 5. Core-shell porous Alg spheres for WAP/Caco2 coculture. A) Schematic illustrating the fabrication of core-shell spheres for WAP and Caco2 coculture. A-i: WAPs suspended in Alg/Cas pre-gel solutions and Caco2 suspended in neutralized decellularized colon matrix were injected into the shell channel and core channel, respectively. 100 mM $CaCl_2$ solutions were used to cross-link core-shell spheres. A-ii: WAP spheroids in the shell part were expected to surround and interact with the core cancer cell aggregates. A-iii: WAPs were labeled by CellTracker™ Green and Caco2 cells were labeled by CellTracker™ Red to indicate their locations in a core-shell sphere. B) SEM image of the acellular core-shell sphere. C) Optical images of core-shell spheres for Caco2 or WAP single cultures or coculture at day 14. D) Live/Dead assay of cells encapsulated in the core-shell particles at day 14. E) BODIPY stained lipids in core-shell spheres after 14 days of single culture or coculture. White dotted lines represent the Caco2 distributions, and purple dotted lines represent the outline of the core-shell spheres. F) Ki67 staining to demonstrate Caco2 proliferation after 14 days of single culture or coculture. G) Glycerol release in the medium of three groups after 14 days culture ($n = 3$). H) Adiponectin secretion in three groups after 14 days of culture ($n = 4$). All quantitative data are expressed as the mean ± standard deviation. Asterisks indicate statistically significant comparisons, with ***$p < 0.001$ and ****$p < 0.0001$, by Student's t-test or one-way ANOVA with Tukey's multiple comparisons tests.

shells, which can result in cellular necrosis in the core, the porous Alg shell with high diffusivity in our current study can ensure sufficient oxygen and nutrient permeability. Most importantly, Alg dissociation allows for the separation and collection of cells within the core and shell regions, enabling us to investigate the impact of the coculture on each cell type.

The 3D printed sphere generation device mentioned above was modified by introducing a core channel inside (**Figure 5**A). Human colorectal adenocarcinoma cells (Caco2) suspended in decellularized porcine colon matrix (characterization was shown in Figure S5, Supporting Information), and WAPs in 50:50 ratio Alg/Cas pre-gel solutions were injected into the core channel

and shell channel of the modified sphere generator, respectively (Figure 5A). Core and shell solution streams were broken into droplets by the air flow simultaneously, which were then quickly cross-linked by the $CaCl_2$ solution. Three groups of core-shell spheres were prepared here: 1) Caco2 group, core: Caco2 in decellularized colon matrix, shell: 50:50 ratio Alg/Cas pre-gel solution without WAPs; 2) WAP group, core: decellularized colon matrix without Caco2, shell: WAPs in 50:50 ratio Alg/Cas pre-gel solution; 3) WAP/Caco2 group, core: Caco2 in decellularized colon matrix, shell: WAPs in 50:50 ratio Alg/Cas pre-gel solution. As demonstrated in Figure 5A, core-shell spheres in direct contact of cancer cells (stained by red cell tracker) with WAPs (stained by green cell tracker) were successfully prepared. By adjusting the flow rate ratio of the core to shell streams, we can control the core volume incorporated in the spheres (Figure S6, Supporting Information). The optical images of core-shell spheres on different days were displayed in Figure S7 (Supporting Information). The SEM image illustrated a porous shell structure and a fibrous core structure (indicated by the red circle and arrows) of acellular core-shell spheres (Figure 5B). We expected that WAP spheroids in porous Alg in the shell would surround and interact with the cancer cell aggregates in the core, recapitulating cellular interactions of tumor and adipocytes in a physiological microenvironment.

After 14 days of culture in the growth medium, the Cas was dissolved, and the core-shell spheres looked transparent (Figure 5C). The single culture of Caco2 was clearly shown in the core of spheres with a transparent shell (Figure 5C). The single culture of WAP and the coculture of WAP/Caco2 illustrated similar morphologies, with distributed WAP spheroids among core-shell spheres (Figure 5C). Due to the high diffusivity and oxygen permeability of the porous Alg shell, our 3D core-shell spheres enabled the cultivation of cells without necrosis. High cell viability was shown in all groups by the Live/Dead assays (Figure 5D).

The biological crosstalk between WAPs and Caco2 during coculture was then investigated. Lipids in WAPs were stained by BODIPY (Figure 5E). Similar to results mentioned above, WAPs in porous Alg shells illustrated auto-differentiation and accumulated plenty of lipids after 14 days of culture. However, a decreased lipid content was observed in WAPs after coculture with Caco2 (Figure 5E). At the same time, the glycerol release from the WAP/Caco2 coculture group was significantly increased compared to the WAP and Caco2 groups (Figure 5G). These results indicated that Caco2 stimulated delipidation of WAPs. An important adipokine, adiponectin, was also quantified. A reduction in adiponectin levels in colorectal cancer patients was reported to be associated with an increase in colon tumor development.[26] However, no significant difference was noticed between the WAP and WAP/Caco2 groups (Figure 5H).

To explore the influence of WAPs on Caco2, Ki67, which is associated with the proliferative activity of malignant cells,[27] was stained. As shown in Figure 5F, much more Ki67 positive nuclei were observed in the Caco2 in the coculture group than in the single culture groups. This indicated that Caco2 proliferation increased when cocultured with WAPs. To investigate protein changes in Caco2 after coculture, core Caco2 was separated from shell WAPs by dissociating the Alg spheres using ethylenediaminetetraacetic acid (EDTA) (Figure S8, Supporting Information). As shown in **Figure 6**A, WAP/Caco2 coculture increased the autophagic flux, which was measured by the significant activation of phosphorylated Unc-51 like autophagy activating kinase (p-ULK1) and the reduction of phosphorylated S6 kinase (p-S6K). The formation of lipidated light chain (LC)3 II from unlipidated LC3 I further confirmed the activation of autophagy in Caco2 in the coculture group. An increase of p62, an autophagic cargo receptor, was shown after WAP/Caco2 coculture, but there was no significant difference (Figure 6A). Autophagy was reported to play an important role in cancer development.[28] Autophagy is protective for tumor initiation, but in tumors, autophagy activation is favorable for cancer cell survival and tumor growth.[29] Autophagy has also been associated with cancer progression, which depends mainly on metastasis dissemination and resistance to anticancer therapies. In this WAP/Caco2 model, we demonstrated that WAPs stimulated cancer cell autophagy and promoted cancer cell survival and proliferation. Our findings showed that Caco2 cells cocultured with WAPs exhibited a significant increase of up to 2-fold in p-ULK1 and a 1.7-fold in LC3 II levels (Figure 6A). These results are comparable to the previous in vivo model where adipocytes and epithelial adenocarcinoma cells were cocultured in NSG (NOD Scid gamma immunodeficient) mice, which showed a 3-times increase in LC3 II levels.[14b] Therefore, our current WAP/Caco2 coculture model holds promise for investigating cell interactions.

Cytokine arrays were then performed to compare protein secretion profiles in coculture and single culture systems (Figure 6B). Seven cytokines were detected only in the WAP/Caco2 coculture group, including insulin-like growth factor-binding protein (IGFBP)-3, leptin, interferon (IFN)-gamma, platelet-derived growth factor (PDGF)-BB, pulmonary and activation-regulated chemokine (PARC), C-X-C motif chemokine ligand (CXCL)-10, and fibroblast growth factor (FGF)-9 (Figure 6C). The secretion of regulated upon activation, normal T cell expressed and secreted (RANTES), oncostatin-M (OSM), vascular endothelial growth factor (VEGF)-A, osteopontin (OPN), and leukemia inhibitory factor (LIF) was increased in WAP/Caco2 coculture group compared to WAP and Caco2 groups (Figure 6C). These increasingly produced cytokines that can be mainly divided into three categories: anticancer or pro-apoptosis, tumor growth, and proinflammatory. IGFBP-3 was reported to be proapoptotic in breast cancer cells, and its release may also indicate the autophagy in the WAP/Caco2 group.[30] PDGF-BB, CXCL-10, and FGF-9 are associated with cellular growth processes, including embryonic development, tissue repair, and tumor growth and invasion.[31] Leptin is one major adipokine secreted by adipocytes and can stimulate the proliferation and migration of cancer cells.[32] Besides its important role on cancer growth and metastasis, the activation of the leptin pathway is also associated with a resistance to therapy of cancer cells.[33] The increased production of leptin was consistent with the proliferation of Caco2 in the coculture group. Proinflammatory cytokines, including IFN-gamma, RANTES, OSM, LIF, and OPN, mediate immunity and function as the activators of macrophages during tumor-adipose interactions.[34] There were also some cytokines without obvious concentration changes after coculture (Figure 6D), including brain-derived neurotrophic factor (BDNF), neurotrophin (NT)-3, tropomyosin-1 (TPM1), IGFBP-2, TMP2, and Interleukin-8 (IL-8). Unlike IGFBP-3, IGFBP-2 was often highly expressed

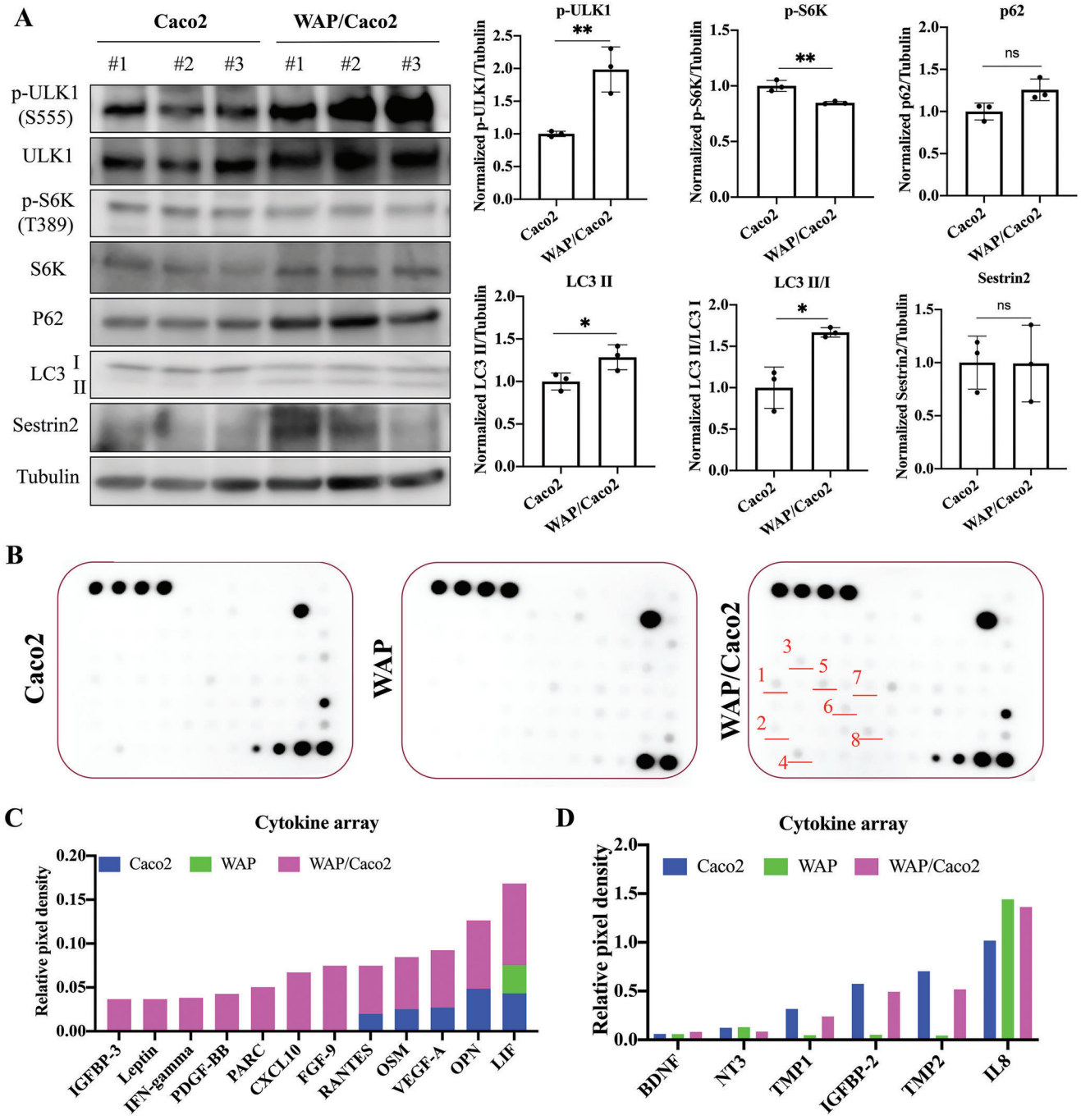

Figure 6. Characterization of WAP/Caco2 crosstalk in core-shell spheres. A) Western blot and its analysis of Caco2 proteins in single culture or coculture with WAP ($n = 3$). B) Cytokine array of three groups after 14 days of culture. 1: OSM, 2: IGFBP-3, 3: RANTES, 4: OPN, 5: VEGF-A, 6: FGF-9, 7: Leptin, 8: LIF. C). Increased cytokine secretion after WAP/Caco2 coculture. D) Unchanged or slightly decreased cytokine secretion after WAP/Caco2 coculture. All quantitative data are expressed as the mean ± standard deviation. Asterisks indicate statistically significant comparisons, with $*p < 0.05$ and $**p < 0.01$, by Student's t-test.

in malignant tumors, and it was shown in similar amounts in the Caco2 and WAP/Caco2 groups (Figure 6D). IL-8 belongs to the proinflammatory cytokines and can be released from cancer cells or isolated adipocytes in vitro.[35] It was observed to have high expressions in all three groups, which may indicate that IL-8 could be involved in some of the adipocyte- or cancer-related complications.

Taken together, core-shell porous Alg spheres were fabricated and worked successfully to coculture WAPs and Caco2. WAPs in the shell region formed spheroids and auto-differentiated,

surrounding the Caco2 aggregates in the decellularized matrix in the core. The crosstalk between them was then investigated. Caco2 was found to stimulate lipid secretion in WAPs after coculture. Meanwhile, WAPs promoted the proliferation and autophagy of Caco2, which was regarded as possible cancer cell survival mechanism. The WAP/Caco2 coculture also resulted in increased secretions of cytokines related to cancer pro-apoptosis, tumor growth, and proinflammation.

The crosstalk between adipose tissue and tumors has received a lot of research interests, and some of the findings are consistent with ours. For instance, previous studies have reported that adipocytes provide adipokines and lipids to cancer cells to promote transformation of benign epithelium, fatty acid metabolism switch in cancer cells, metastases, and chemoresistance.[13] Adipose tissue is a complex environment composed of adipocytes, progenitors, and immune cells, storing and releasing energy in response to physiological demands. The tumorigenesis process can be promoted by adipose dysfunction and chronic inflammation or paracrine factors secreted by stromal and immune cells in adipose tissues.[36] Adipose tissue also functions as an endocrine organ, secreting adipokines, the altered secretion of which has been found to correlate with cancer aggressiveness. During cancer progression, tumor cells undergo metabolic symbiosis with adjacent adipose tissues. Cancer cells experience metabolic reprogramming to increase their utilization of lipids in hypoxic conditions,[37] while adipocytes undergo lipolysis and serve as a source of lipids for cancer cells.[38] There is also emerging evidence showing that adipose tissue-derived cells and factors contribute to the therapy resistance of various cancers, which is in part due to the changes in the tumor matrix driven by the adipose tissue. Adipose tissue creates a microenvironment that supports proliferation and resistance to chemotherapy for disseminating leukemia cells. More detailed discussions on adipocyte and cancer cell crosstalk can be found in a review paper.[13]

Although promising, our current WAP/Caco2 coculture model has its limitations. Even though we illustrated that WAPs could auto-differentiate without differentiation medium treatment in porous Alg spheres, they did not completely mature to adipocytes. To better mimic the crosstalk of adipose tissues and tumors while avoiding side effects of differentiation medium on Caco2, the utilization of stem cells/progenitor cells combined with pre-differentiation can possibly result in more mature adipocytes and thus more efficient disease modeling. However, the WAPs in our current work, as model cells for proof-of-concept, suffered from limited survival once encapsulated after differentiation. In addition, as a cancer cell survival mechanism, autophagy in Caco2 was observed when cocultured with WAPs. We speculated that some molecules from WAPs (i.e., secretory autophagy proteins, functional RNAs) might be secreted and uptaken by Caco2 cells to activate autophagy. Therefore, the analysis on secretory autophagy molecules, adipose derived exosome or micro-vesicles, and secreted free fatty acid in medium can be conducted in future studies.

3. Conclusion

In summary, we have described a simple and biocompatible method for preparing porous cell-laden Alg hydrogels based on aqueous two-phase emulsions using a blend of Alg and Cas solutions. The pore sizes, rheological properties, and macromolecule diffusion abilities of the hydrogel constructs were characterized to obtain the optimal combination of the desired structural integrity along with porous structures. The heterogeneous pores, interconnected paths, and bioinert matrix of porous Alg hydrogels facilitated encapsulated WAP survival, proliferation, in situ spheroid organization, and adipogenic differentiation, compared to conventional non-porous Alg hydrogels. The feasibility of porous Alg hydrogels for use in applications in WAP/Caco2 coculture was demonstrated in core-shell spheres, with WAP clusters distributed around Caco2 aggregates. These results collectively suggest that our facile approach for generating porous Alg hydrogels provides a promising platform for use as a cell carrier and in disease modeling.

4. Experimental Section

Alg/Cas Emulsion Preparation and Characterization: Alg powder (Protanal LF 10/60 FT, FMC Corporation) and Cas powder (C8654, Sigma-Aldrich) were mixed and dissolved in saline solutions by stirring overnight at room temperature to prepare Alg/Cas emulsions. The final concentration of Alg in the mixture was 2%, and the concentration of Cas was 1%, 3%, or 5%. A brightfield microscope (DMi1, Leica) was used to visualize the incompatibility and phase separation of Alg and Cas in the mixed solutions. The viscosities of mixtures with varying Cas concentrations were evaluated through a rheometer (HR-2, TA Instruments) at a shear rate from 1 to 10 000 1/s.

To separate two incompatible phases in Alg/Cas emulsions, they were centrifuged at 10 000 g for 3 h at room temperature. The top and bottom phases were each collected separately and stored at 4 °C for further use. To determine the composition of the separated top and bottom phases, a Pierce™ BCA Protein Assay Kit (Thermo Scientific) was applied to test the Cas concentrations. For Alg concentration measurement, the law of Conservation of Mass was applied. Briefly, 2 mL of the top and bottom solutions were each freeze-dried and weighed. The amount of Alg was calculated by deducting the amount of Cas from the total mass in each phase.

Porous Alg Hydrogel Fabrication and Characterization: For the preparation of the pre-gel solution, the top phase (Alg-rich phase) and bottom phase (Cas-rich phase) obtained from centrifugation were mixed thoroughly in ratios of 0:100, 10:90, 30:70, 50:50, 70:30, 90:10, and 100:0 (v/v). Two percent Alg was used as the control solution. Brightfield images were taken to evaluate phase separation of the Alg/Cas pre-gel solutions. Alg was then labeled with tetramethylrhodamine cadaverine, according to previous reported protocols.[39] The pre-gel solutions with different top/bottom volume ratios were imaged by a CLSM (LSM 710, Zeiss). The droplet sizes of the emulsions in pre-gel solutions were measured by ImageJ software according to CLSM images.

Pre-gel solutions with the different top/bottom volume ratios prepared above were added into self-made agarose molds (3 mm in height and 6 mm in diameter). Agarose powder (12 mg mL^{-1}, Sigma-Aldrich) was dissolved in 100 mM boiled $CaCl_2$ solutions (Sigma-Aldrich). After cooling at room temperature, agarose molds were made by using 6 mm diameter punches. Calcium ions in the agarose molds diffused slowly to cross-link Alg in the pre-gel solutions. After cross-linking at room temperature for 1 h, the hydrogels were collected. The inner porous structures of obtained Alg hydrogels were then examined under a CLSM, with Alg conjugated by tetramethylrhodamine cadaverine. Their pore sizes were measured through ImageJ software. After lyophilization, the microstructures of the porous hydrogels were investigated with SEM (FEI Quanta 200) at 10 kV.

To evaluate the Cas leaching process, hydrogels were immersed in deionized water (DI) at 37 °C for 7 days. The water was changed every 24 h. The released Cas concentration was measured by a Pierce™ BCA Protein Assay Kit.

The mechanical properties of the different hydrogel constructs were measured by a rheometer with a gap of 500 µm and a plate diameter of 20 mm. Both an oscillation strain sweep (0.01–10% strain, 1 rad s^{-1}) and a frequency sweep (0.1–100 rad s^{-1}, 1% strain) were conducted. The storage modulus (G') and loss modulus (G'') were recorded and compared.

The diffusive performance of hydrogels with macromolecules was tested by dropping FITC-conjugated-dextran solutions onto the top surface of hydrogel cylinders. In brief, hydrogel cylinders (6 mm in diameter and 5 mm in thickness) were placed separately on a piece of clean filter paper. The FITC-conjugated-dextran (40 kDa, Sigma-Aldrich) (1%, 10 µL) was dropped onto the surface of each hydrogel cylinder. The diffusion of dextran through the hydrogels was recorded under the excitation of ultraviolet radiation (UV) (OmniCure S2000 UV lamp, 365 nm) after 3 min by using a digital camera. Similar tests were also conducted by dropping bovine serum albumin solutions (BSA, 1%) mixed with red dye onto the surface of the hydrogel cylinders, which were placed on a petri dish.

WAP-Laden Porous Alg Hydrogel Fabrication: Immortalized human WAPs were a generous gift from Dr. Yu-Hua Tseng at the Joslin Diabetes Center, Harvard Medical School. The WAPs were generated by isolating primary stromal vascular cells from the subcutaneous fat of an anonymous female, and subsequently infected with retrovirus expressing human telomere reverse transcriptase (hTERT).[40] The WAPs were cultured in a growth medium containing Dulbecco's Modified Eagles Medium (DMEM/high glucose), 10% fetal bovine serum (FBS, Gibco), and 1% penicillin/streptomycin (P/S, Gibco) in 5% CO_2 at 37 °C.

WAPs were digested and resuspended in pre-gel solutions at a density of 5×10^6 cells mL^{-1}. Cell-laden pre-gel solutions were then cross-linked in agarose molds, as mentioned above, for 1 h in an incubator (5% CO_2, 37 °C). Afterward, these cell-loaded hydrogel constructs were cultured in WAP growth medium for 7 days, with medium being changed every day.

The cell viability was examined by a Live/Dead assay (Invitrogen). Images of the Live/Dead assays were taken by the LSM 710. The areas of cells or cell clusters in different hydrogels were measured by ImageJ software according to the Live/Dead images at days 3 and 7. Brightfield images of WAP-laden hydrogels at day 7 were also recorded. The constructs were then fixed in 4% paraformaldehyde (PFA) for 1 h, dehydrated in 30% sucrose overnight, embedded into optimal cutting temperature (OCT, Fisher HealthCare) compound, and cut into 10 µm sections for H&E staining. Besides morphological evaluations, the proliferation of cells encapsulated in different hydrogels was measured spectrophotometrically at days 3 and 7 by using a 3-(4,5-dimethyl-2-thiazolyl)-2,5-diphenyl-2H-tetrazolium bromide assay (MTT, Sigma-Aldrich). The absorbance values were read at 570 nm.

Fabrication and Characterization of Porous Alg Spheres with Encapsulated WAPs: Production of porous Alg spheres was performed on this formerly reported sphere generation device.[23] Briefly, pre-gel solutions were injected through the syringe into a self-designed bead generator at a flow rate of 0.3 mL min^{-1}. The injected solution stream was continuously cleaved into droplets by an air flow (10 L min^{-1}), which were then collected and cross-linked in 100 mM $CaCl_2$ solution. The morphology of acellular spheres was observed by a darkfield microscope (Leica). Their inner porous structure was investigated by the SEM at 10 kV after lyophilization and sputter coating.

For Alg spheres with encapsulated WAPs, the WAPs were suspended into pre-gel solutions (5×10^6 cells mL^{-1}) and followed the same fabrication method as mentioned above. WAP-laden spheres were cultured in WAP growth medium in an incubator for 7 days and were imaged by a brightfield microscope. The viability of the encapsulated cells was examined by a Live/Dead assay at day 7. The proliferation of cells was tested by MTT assays at days 3 and 7. WAP-laden spheres were then differentiated, as mentioned before.[41] The spheres were first cultured in a differentiation medium consisting of DMEM/high glucose with 2% FBS, 1% P/S, 0.5 µM recombinant human insulin (Alfa Aesar), and 2 nM triiodothyronine (T3, Sigma-Aldrich) for 6 days, with the medium changed every 3 days. Induction was further conducted for another 12 days with an induction medium that consisted of the differentiation medium plus 33 µM biotin (Sigma-Aldrich), 17 µM pantothenate (Sigma-Aldrich), 0.1 µM dexamethasone (Sigma-Aldrich), 500 µM 3-isobutyl-1-methyl xanthine (IBMX, Sigma-Aldrich), and 30 µM indomethacin (Sigma-Aldrich). The medium was changed every 3 days. For Alg spheres without differentiation, they were cultured in the WAP growth medium for the same amount of time.

After that, intracellular lipid accumulation in Alg spheres was quantitatively determined enzymatically using Free Glycerol Reagent (F6428, Sigma-Aldrich) and Triglyceride Reagent (T2449, Sigma-Aldrich). Briefly, WAP-laden spheres with or without differentiation were added into sodium dodecyl sulfate buffer (0.1% w/v). They were homogenized by pipetting the mixture up and down, followed by sonication for 10 min. The supernatants were collected after centrifugation at 15 000 g for 10 min at 4 °C. The quantification of the triglyceride concentration was carried out according to the manufacturer's instructions and recorded with a plate reader at 570 nm. Triglyceride concentrations from each group were normalized to the total amount of DNA in the respective sphere lysates tested by the Quant-iT™ PicoGreen dsDNA Reagent (Invitrogen).

To image the accumulated lipids, 10 µg mL^{-1} of BODIPY™ 493/503 (D3922, Thermo Fisher Scientific) and DAPI (1:1000) in saline solutions were added and incubated with the Alg spheres for 30 min at room temperature. Images were taken by the 710 CLSM. Oil Red O staining was also conducted after Alg spheres were sectioned into 10 µm slices. Slides were incubated in Oil Red O working solutions for ≈10 min. Hematoxylin was then added to stain the cell nucleus.

Immunohistochemical (IHC) staining of collagen I was conducted to detect the ECM in different groups. To stain collagen I, slides were pre-incubated with 3% hydrogen peroxide for 10 min to deactivate the endogenous peroxidase and then blocked with blocking serum for 1 h at room temperature. The sections were then incubated overnight at 4 °C with anti-collagen type I primary antibodies (Col I, NB600-408, Novus Biologicals). After washing them three times with PBS, biotinylated goat anti-rabbit IgG (1:150, Vector Laboratories) was added and cultured for 30 min at room temperature. After washing them with PBS, avidin-biotin complex conjugated to peroxidase (Vector Laboratories) was applied for 30 min. The bound complexes were visualized by adding DAB substrate (3,3'-diaminobenzidine, Vector Laboratories) to the sections for 5 min.

Fabrication of Core-Shell Spheres and their Applications in WAP/Caco2 Coculture: The bead generation device in Section 4.4 was modified by introducing a core channel to produce core-shell Alg spheres for coculturing WAPs and cancer cells. Human colorectal adenocarcinoma cells, Caco2 (originally purchased from ATCC), were a kind gift from Dr. Jennifer Black at The University of Nebraska Medical Center. They were expanded in growth medium consisting of DMEM/high glucose, 10% FBS, and 1% P/S in 5% CO_2 at 37 °C. Caco2 cells were then suspended in decellularized porcine colon solution. Fresh porcine colons were bought from Nebraska Scientific (Nebraska, United States) and decellularized according to previous methods that were based on combined chemical and enzymatic agents.[42] Briefly, fresh porcine colons were stirred in 50 mM Tris buffer (pH = 8) overnight and then in 1% Triton-X 100 in 50 mM Tris buffer solution at 4 °C for 24 h. This was followed by 40 units mL^{-1} of DNase (0 453 628 2001, Roche), 20 mg L^{-1} of RNase (R4875, Sigma-Aldrich), and 0.01% Trypsin (Sigma-Aldrich) in Hank's Balanced Salt Solution (HBSS) for 4 h at 37 °C. Finally, they were stirred overnight in 1% Triton-X 100 in 50 mM Tris buffer at 4 °C. Histological sections and H&E staining were performed to verify the decellularization results. Native colons and decellularized colons were fixed in 10% formalin buffer for 4 h. After washing them with PBS thrice, they were embedded in paraffin, sectioned, and stained by H&E. The DNA, collagen, and glycosaminoglycan (GAG) concentrations were also determined after decellularization according to previous methods.[42] After lyophilization, the decellularized colons were cut into small pieces and digested in 1 mg mL^{-1} pepsin (Sigma-Aldrich) in 0.01 N HCl solution (10 mg mL^{-1} decellularized colons). After constant agitation for 48 h at room temperature, the solution was neutralized by 1 N sodium hydroxide (NaOH, Fisher Chemical) and 10 × PBS (1/10 of the final volume).

WAPs (5×10^6 cells mL^{-1}) were suspended in Alg/Cas pre-gel solutions and injected into the shell channel of the modified bead generator at a flow rate of 0.5 mL min^{-1}. Caco2 cells suspended in neutralized

decellularized colon matrix solution were injected into the core channel at the flow rate of 0.13 mL min^{-1}. The injected core and shell solution streams were cleaved into droplets simultaneously by an air flow (10 L min^{-1}), which then fell into 100 mM $CaCl_2$ solution and were cross-linked. WAPs were labeled by CellTracker™ Green CMFDA (ThermoFisher), and Caco2 cells were labeled by CellTracker™ Red CMTPX (ThermoFisher) to indicate their locations in a core-shell sphere. To evaluate the microstructures of the core-shell spheres, SEM was conducted on acellular spheres. Core-shell Alg spheres with WAPs and Caco2 cells were cultured in growth medium (DMEM/high glucose, 10% FBS, and 1% P/S) for 14 days. Optical images of them were taken, and the viability was examined by the Live/Dead assay at day 14.

Characterization of the Crosstalk between WAPs and Caco2 Cells: The biological crosstalk between WAPs and Caco2 cells in coculture was studied. To investigate the influence of the crosstalk on WAPs, their lipids were stained by BODIPY as mentioned above. The growth medium in the three groups was not changed from days 12 to 14, and the supernatants were collected afterward. The glycerol release was then tested by a Glycerol Assay Kit (MAK117, Sigma-Aldrich), and the adiponectin secretion was measured by a Human Total Adiponectin/Acrp30 Quantikine ELISA (DRP300, R&D Systems).

Caco2 proliferation in single culture and coculture was observed through Ki67 immunofluorescence staining. Briefly, core-shell spheres were fixed in 4% PFA for 1 h. Nonspecific antibody binding was blocked by 5% goat serum solution, followed by overnight incubation at 4 °C with a primary Ki67 antibody in 0.04% Triton X-100 and 5% goat serum. Then corresponding secondary antibodies were added and incubated for 2 h at room temperature. The samples were imaged by 710 CLSM after nuclear staining with DAPI for 10 min. Caco2 in a decellularized matrix from the core-shell spheres was separated after Alg dissociation by EDTA solution (4 mM EDTA + 0.15 M sodium chloride, pH = 7.4) for 30 min on ice. Caco2 aggregates were then collected by centrifugation (300 rpm, 3 min). Immunoblotting was performed to detect the protein expressions of cancer cells in the Caco2 and WAP/Caco2 groups. Primary antibodies to detect p-UKL1 S555 (5869S), UKL1 (4773S), p-S6K T389 (9205), S6K (9202), SQSTM1/P62 (5114), LC3 (3868) were from Cell Signaling Technology. Anti-Sestrin2 (10795-1-AP) antibody was from Proteintech. Anti-Tubulin was from Developmental Studies Hybridoma Bank. Cell lysates prepared in cell lysis buffer (20 mM Tris-Cl pH 7.5, 150 mM NaCl, 1 mM EDTA, 1 mM EGTA, 2.5 mM sodium pyrophosphate, 1 mM β-glycerophosphate, 1 mM Na3VO4, 1% Triton-X-100, 0.1% SDS) contained protease inhibitor cocktail (Roche) and phosphatase inhibitor (Sigma). The immunocomplexes and enzymatic reaction mixtures were boiled in SDS sample buffer for 5 min, separated by SDS-PAGE, transferred to PVDF membranes and probed with primary antibodies. After incubation with secondary antibodies conjugated with HRP, chemiluminescence was detected using Odyssey Clx imaging system (LI-COR Biosciences, Lincoln, NE). The relative protein expression was analyzed using ImageJ software and normalized to control Tubulin.

The relative amounts of cytokines in Caco2, WAP, and WAP/Caco2 supernatants (days 12 to 14) were evaluated by a Human Cytokine Array C5 (AAH-CYT-5-4, RayBiotech), following the manufacturer's protocol. Briefly, 1 mL of the supernatant was mixed with a cocktail of biotinylated detection antibodies and incubated with the array membrane overnight at 4 °C. After washing it, streptavidin-horseradish peroxidase solution and chemiluminescent detection reagents were added to the membrane in sequence. Then the array membranes were imaged and scanned. The pixel density of each dot was analyzed with ImageJ software and normalized to positive controls.

Statistical Analysis: All quantitative data were expressed as the mean ± standard deviation (SD). A statistical analysis was also performed. In experiments with two groups, student t-tests were used, while in experiments with more than two groups, one-way analysis of variance ANOVA was used with Tukey post-hoc tests for statistical analysis. Differences with $p < 0.05$ were denoted as *, while $p < 0.01$ was denoted as **, $p < 0.001$ was denoted as ***, $p < 0.0001$ was denoted as ****, and *ns* indicated not significant.

Supporting Information

Supporting Information is available from the Wiley Online Library or from the author.

Acknowledgements

This work was supported by University of Nebraska Collaboration Initiative Grant (B.D.). This work was supported by Undergraduate Creative Activities and Research Experience (UCARE) program-scholarship from the Pepsi Quasi Endowment and Union Bank & Trust to T.K., University of Nebraska Initiative Team Seed grant to S.-H.R. This research was supported in part by funding from the National Institute of General Medical Sciences of the National Institute of Health under Award Number (P20GM104320).

Conflict of Interest

The authors declare no conflict of interest.

Author Contributions

W.X. and B.D. conceived the study idea. W.X., S.R., and B.D. designed the experiments. W.X. conducted experiments, wrote the manuscript, and revised the manuscript. D.L. and M.K. designed and prepared the sphere generation device. T.K. and S.R. performed the western blot and conducted its analysis. Y. H. helped with the cytokine array. All authors contributed to discussing the results and implications and editing the manuscript.

Data Availability Statement

The data that support the findings of this study are available from the corresponding author upon reasonable request.

Keywords

adipose-cancer interaction, core-shell, porous hydrogels, spheroids, two-phase aqueous emulsions

Received: December 3, 2022
Revised: April 5, 2023
Published online:

[1] a) W. R. Gombotz, S. Wee, *Adv. Drug Delivery Rev.* **1998**, *31*, 267; b) K. Y. Lee, D. J. Mooney, *Prog. Polym. Sci.* **2012**, *37*, 106.
[2] R. K. Kankala, J. Zhao, C. G. Liu, X. J. Song, D. Y. Yang, K. Zhu, S. B. Wang, Y. S. Zhang, A. Z. Chen, *Small* **2019**, *15*, 1901397.
[3] a) B. V. Slaughter, S. S. Khurshid, O. Z. Fisher, A. Khademhosseini, N. A. Peppas, *Adv. Mater.* **2009**, *21*, 3307; b) L. Ma, A. Gaisinskaya-Kipnis, N. Kampf, J. Klein, *Nat. Commun.* **2015**, *6*, 6060; c) T. Shoaib, J. Heintz, J. A. Lopez-Berganza, R. Muro-Barrios, S. A. Egner, R. M. Espinosa-Marzal, *Langmuir* **2018**, *34*, 756; d) E. M. Johnson, W. M. Deen, *AIChE J.* **1996**, *42*, 1220.
[4] K. J. De France, F. Xu, T. Hoare, *Adv. Healthcare Mater.* **2018**, *7*, 1700927.
[5] a) N. Huebsch, E. Lippens, K. Lee, M. Mehta, S. T. Koshy, M. C. Darnell, R. M. Desai, C. M. Madl, M. Xu, X. Zhao, *Nat. Mater.* **2015**, *14*, 1269; b) G. L. Ying, N. Jiang, S. Maharjan, Y. X. Yin, R. R. Chai, X. Cao, J. Z. Yang, A. K. Miri, S. Hassan, Y. S. Zhang, *Adv. Mater.* **2018**, *30*, 1805460.

[6] a) M. Dvir-Ginzberg, T. Elkayam, S. Cohen, *FASEB J.* **2008**, *22*, 1440; b) T. Andersen, P. Auk-Emblem, M. Dornish, *Microarrays* **2015**, *4*, 133.
[7] a) P. Zhuang, A. X. Sun, J. An, C. K. Chua, S. Y. Chew, *Biomaterials* **2018**, *154*, 113; b) P. Zhuang, Y.-H. Chiang, M. S. Fernanda, M. He, *Int. J. Bioprint* **2021**, *7*, 444.
[8] a) C. M. Hwang, S. Sant, M. Masaeli, N. N. Kachouie, B. Zamanian, S.-H. Lee, A. Khademhosseini, *Biofabrication* **2010**, *2*, 035003; b) A. Sergeeva, N. Feoktistova, V. Prokopovic, D. Gorin, D. Volodkin, *Adv. Mater. Interfaces* **2015**, *2*, 1500386; c) A. Sergeeva, A. S. Vikulina, D. Volodkin, *Micromachines* **2019**, *10*, 357; d) H. Zhao, X.-K. Ouyang, L.-Y. Yang, *J. Mol. Liq.* **2021**, *324*, 115122.
[9] a) S. Partap, I. Rehman, J. R. Jones, J. A. Darr, *Adv. Mater.* **2006**, *18*, 501; b) S. Partap, A. Muthutantri, I. Rehman, G. Davis, J. Darr, *J. Mater. Sci.* **2007**, *42*, 3502.
[10] a) P. Eiselt, J. Yeh, R. K. Latvala, L. D. Shea, D. J. Mooney, *Biomaterials* **2000**, *21*, 1921; b) A. Barbetta, E. Barigelli, M. Dentini, *Biomacromolecules* **2009**, *10*, 2328; c) S. A. Siboro, D. S. Anugrah, K. Ramesh, S.-H. Park, H.-R. Kim, K. T. Lim, *Carbohydr. Polym.* **2021**, *260*, 117779.
[11] a) N. Annabi, J. Nichol, X. Zhong, C. Ji, S. Koshy, A. Khademhosseini, F. Dehghani, *Tissue Eng., Part B* **2010**, *16*, 371; b) K. Kabiri, H. Omidian, M. Zohuriaan-Mehr, *Polym. Int.* **2003**, *52*, 1158.
[12] a) A. Mondal, A. Gebeyehu, M. Miranda, D. Bahadur, N. Patel, S. Ramakrishnan, A. K. Rishi, M. Singh, *Sci. Rep.* **2019**, *9*, 19914; b) S. B. Park, B. Koh, W. H. Jung, K. J. Choi, Y. J. Na, H. M. Yoo, S. Lee, D. Kang, D. M. Lee, K. Y. Kim, *Diabetes, Obes. Metab.* **2020**, *22*, 1302; c) N. Chaicharoenaudomrung, P. Kunhorm, P. Noisa, *World J. Stem Cells* **2019**, *11*, 1065; d) Y.-C. E. Li, Y. A. Jodat, R. Samanipour, G. Zorzi, K. Zhu, M. Hirano, K. Chang, A. Arnaout, S. Hassan, N. Matharu, *Biofabrication* **2020**, *13*, 015014.
[13] E. Lengyel, L. Makowski, J. DiGiovanni, M. G. Kolonin, *Trends Cancer* **2018**, *4*, 374.
[14] a) K. M. Nieman, I. L. Romero, B. Van Houten, E. Lengyel, *Biochim. Biophys. Acta* **2013**, *1831*, 1533; b) Y.-A. Wen, X. Xing, J. W. Harris, Y. Y. Zaytseva, M. I. Mitov, D. L. Napier, H. L. Weiss, B. M. Evers, T. Gao, *Cell Death Dis.* **2017**, *8*, 2593.
[15] J. Yamaguchi, H. Ohtani, K. Nakamura, I. Shimokawa, T. Kanematsu, *Am. J. Clin. Pathol.* **2008**, *130*, 382.
[16] a) D. Chen, S. Liu, H. Ma, X. Liang, H. Ma, X. Yan, B. Yang, J. Wei, X. Liu, *Cancer Cell Int.* **2015**, *15*, 42; b) S. Balaban, R. F. Shearer, L. S. Lee, M. van Geldermalsen, M. Schreuder, H. C. Shtein, R. Cairns, K. C. Thomas, D. J. Fazakerley, T. Grewal, J. Holst, D. N. Saunders, A. J. Hoy, *Cancer Metab.* **2017**, *5*, 1; c) F. Preisner, U. Leimer, S. Sandmann, I. Zoernig, G. Germann, E. Koellensperger, *Stem Cell Rev. Rep.* **2018**, *14*, 125.
[17] a) Y. Tokuda, Y. Satoh, C. Fujiyama, S. Toda, H. Sugihara, Z. Masaki, *BJU Int.* **2003**, *91*, 716; b) S. Chaji, J. Al-Saleh, C. T. Gomillion, *Gels* **2020**, *6*, 10; c) J. Seo, K. S. Kim, J.-W. Park, J.-Y. Cho, H. Chang, J. Fukuda, K. Y. Hong, Y.-S. Chun, *Biomaterials* **2021**, *269*, 120622.
[18] W. Chen, S. Zhou, L. Ge, W. Wu, X. Jiang, *Biomacromolecules* **2018**, *19*, 1732.
[19] L. Léonard, A. Gharsallaoui, F. Ouaali, P. Degraeve, Y. Waché, R. Saurel, N. Oulahal, *Colloids Surf., B* **2013**, *109*, 266.
[20] N. Broguiere, A. Husch, G. Palazzolo, F. Bradke, S. Madduri, M. Zenobi-Wong, *Biomaterials* **2019**, *200*, 56.
[21] a) Z. Cesarz, K. Tamama, *Stem Cells Int.* **2016**, *2016*, 9176357; b) S. Sart, A.-C. Tsai, Y. Li, T. Ma, *Tissue Eng., Part B* **2014**, *20*, 365; c) R. O. Hynes, *Nat. Rev. Mol. Cell Biol.* **2014**, *15*, 761.
[22] K. M. Z. Hossain, U. Patel, I. Ahmed, *Prog. Biomater.* **2015**, *4*, 1.
[23] D. Lee, S. E. Greer, M. A. Kuss, Y. An, A. T. Dudley, *Biomed. Microdevices* **2021**, *23*, 22.
[24] N. P. Visavadiya, G. S. Pena, A. V. Khamoui, *Mol. Cell. Biochem.* **2021**, *476*, 23.
[25] M. Tabuso, S. Homer-Vanniasinkam, R. Adya, R. P. Arasaradnam, *World J. Gastroenterol.* **2017**, *23*, 5829.
[26] W. An, Y. Bai, S.-X. Deng, J. Gao, Q.-W. Ben, Q.-C. Cai, H.-G. Zhang, Z.-S. Li, *Eur. J. Cancer Prev.* **2012**, *21*, 126.
[27] L. T. Li, G. Jiang, Q. Chen, J. N. Zheng, *Mol. Med. Rep.* **2015**, *11*, 1566.
[28] S. Rao, L. Tortola, T. Perlot, G. Wirnsberger, M. Novatchkova, R. Nitsch, P. Sykacek, L. Frank, D. Schramek, V. Komnenovic, *Nat. Commun.* **2014**, *5*, 3056.
[29] A. M. Strohecker, J. Y. Guo, G. Karsli-Uzunbas, S. M. Price, G. J. Chen, R. Mathew, M. McMahon, E. White, *Cancer Discovery* **2013**, *3*, 1272.
[30] a) S. M. Firth, R. C. Baxter, *Endocr. Rev.* **2002**, *23*, 824; b) A. Subramanian, A. Sharma, K. Mokbel, *Breast Cancer Res. Treat.* **2008**, *107*, 181.
[31] M. Kim, H. Y. Choi, J. W. Woo, Y. R. Chung, S. Y. Park, *Sci. Rep.* **2021**, *11*, 18007.
[32] J.-F. Dumas, L. Brisson, *Cancer Metastasis Rev.* **2021**, *40*, 31.
[33] M. Chi, J. Chen, Y. Ye, H.-Y. Tseng, F. Lai, K. H. Tay, L. Jin, S. Guo, C. Jiang, X. Zhang, *Curr. Med. Chem.* **2014**, *21*, 1255.
[34] H. Zhao, Q. Chen, A. Alam, J. Cui, K. C. Suen, A. P. Soo, S. Eguchi, J. Gu, D. Ma, *Cell Death Dis.* **2018**, *9*, 356.
[35] J. M. Bruun, S. B. Pedersen, B. Richelsen, *J. Clin. Endocrinol. Metab.* **2001**, *86*, 1267.
[36] J. Park, T. S. Morley, M. Kim, D. J. Clegg, P. E. Scherer, *Nat. Rev. Endocrinol.* **2014**, *10*, 455.
[37] W. Palm, C. B. Thompson, *Nature* **2017**, *546*, 234.
[38] H. Ye, B. Adane, N. Khan, T. Sullivan, M. Minhajuddin, M. Gasparetto, B. Stevens, S. Pei, M. Balys, J. M. Ashton, D. J. Klemm, C. M. Woolthuis, A. W. Stranahan, C. Y. Park, C. T. Jordan, *Cell Stem Cell* **2016**, *19*, 23.
[39] W. Xue, B. Liu, H. Zhang, S. Ryu, M. Kuss, D. Shukla, G. Hu, W. Shi, X. Jiang, Y. Lei, *Acta Biomater.* **2022**, *138*, 182.
[40] R. Xue, M. D. Lynes, J. M. Dreyfuss, F. Shamsi, T. J. Schulz, H. Zhang, T. L. Huang, K. L. Townsend, Y. Li, H. Takahashi, L. S. Weiner, A. P. White, M. S. Lynes, L. L. Rubin, L. J. Goodyear, A. M. Cypess, Y.-H. Tseng, *Nat. Med.* **2015**, *21*, 760.
[41] W. Xue, S.-Y. Yu, M. Kuss, Y. Kong, W. Shi, S. Chung, S.-Y. Kim, B. Duan, *Biofabrication* **2022**, *14*, 034106.
[42] W. Xue, Y. Kong, R. Abu, P. Roy, S.-H. Huh, M. Kuss, V. Kumar, B. Duan, *ACS Appl. Mater. Interfaces* **2022**, *14*, 8693.